Oceanologia (2016) 58, 71—89

Available online at www.sciencedirect.com

ScienceDirect

journal homepage: www.elsevier.com/locate/oceano

ORIGINAL RESEARCH ARTICLE

An integrated wave modelling framework for extreme and rare events for climate change in coastal areas — the case of Rethymno, Crete☆

Vasiliki K. Tsoukala [a,*], Michalis Chondros [a], Zacharias G. Kapelonis [b], Nikolaos Martzikos [a], Archodia Lykou [c], Kostas Belibassakis [b], Christos Makropoulos [c]

[a] *Laboratory of Harbor Works, National Technical University of Athens, Athens, Greece*
[b] *School of Naval Architecture and Marine Engineering, National Technical University of Athens, Athens, Greece*
[c] *Laboratory of Hydrology & Water Resources Utilization, National Technical University of Athens, Athens, Greece*

Received 23 July 2015; accepted 8 January 2016
Available online 29 January 2016

KEYWORDS
Climate change;
Wave run-up;
Wave overtopping;
Storm events;
Coastal flooding

Summary Coastal floods are regarded as among the most dangerous and harmful of all natural disasters affecting urban areas adjacent to the shorelines. Rapid urbanization combined with climate change and poor governance often results in significant increase of flood risk, especially for coastal communities. Wave overtopping and wave run-up are the key mechanisms for monitoring the results of coastal flooding and as such, significant efforts are currently focusing on their predicting. In this paper, an integrated methodology is proposed, accounting for wave overtopping and wave run-up under extreme wave scenarios caused by storm surges. By taking advantage of past and future climatic projections of wind data, a downscaling approach is proposed,

☆ The research leading to these results has received funding from the European Union Seventh Framework Programme (FP7/2007-2013) under Grant agreement n° 603663 for the research project PEARL (Preparing for Extreme And Rare events in coastaL regions). The research and its conclusions reflect only the views of the authors and the European Union is not liable for any use that may be made of the information contained herein.

* Corresponding author at: Laboratory of Harbor Works, School of Civil Engineering, NTUA, 5, Iroon Polytechniou St., 15780 Zografou, Greece. Tel.: +30 693 246 0540; fax: +30 210 772 2372.
E-mail addresses: vtsouk@hydro.civil.ntua.gr (V.K. Tsoukala), chondros@hydro.ntua.gr (M. Chondros), zkapel@central.ntua.gr (Z.G. Kapelonis), nmartzikos@central.ntua.gr (N. Martzikos), alykou@central.ntua.gr (A. Lykou), kbel@fluid.mech.ntua.gr (K. Belibassakis), cmakro@chi.civil.ntua.gr (C. Makropoulos).

Peer review under the responsibility of Institute of Oceanology of the Polish Academy of Sciences.

ELSEVIER Production and hosting by Elsevier

http://dx.doi.org/10.1016/j.oceano.2016.01.002

utilizing a number of appropriate numerical models than can simulate the wave propagation from offshore up to the swash zone. The coastal zone of Rethymno in Greece is selected as a case study area and simulations of wave characteristics with the model SWAN for the period 1960–2100 in the offshore region are presented. These data are given as boundary conditions to further numerical models (MIKE21 PMS and HD) in order to investigate the spatial evolution of the wave and the hydrodynamic field in intermediate and shallow waters. Finally, the calculated wave height serves as input to empirical formulas and time dependent wave propagation models (MIKE21 BW) to estimate the wave run-up and wave overtopping (EurOtop). It is suggested that the proposed procedure is generic enough to be applicable to any similar region.

1. Introduction

In recent years research efforts from several disciplines have focused on the long-term prediction of climate change and its effects, including prediction of wind and wave climate changes, intensity and frequency of rainfalls as well as changes in temperature and increase in sea level. This paper focuses on the effects of climate change on coastal zones and specifically examines the occurrence of coastal floods under climate change scenarios.

Coastal floods are complex phenomena influenced by a series of factors including the bathymetry of sea bottom, existing port and coastal works, erosion and sea level rise phenomena geometry of the urban environments (e.g. roads, buildings, drainage systems, etc.). Recent research has contributed to the development of useful tools to predict and calculate the causes of coastal flood events (Kundzewicz, 2014) arising from e.g. storms and storm surges (Anselme et al., 2011; Breilh et al., 2014; Long et al., 2014), sea level rise (Warner and Tissot, 2012; Wiśniewski and Wolski, 2011) and tsunami (McCabe et al., 2014). These phenomena eventually result in wave overtopping and wave run-up (Laudier et al., 2011; Lynett et al., 2010; Matias et al., 2012; Plant and Stockdon, 2015; Senechal et al., 2011; Smith et al., 2012; Stockdon and Holman, 2011) on shore and thus result in coastal flooding. During the last years the impacts of climate change on coastal flooding and on the stability and operation of ports and coastal defense structures has risen in attention, looking specifically on disaster risk resilience (Karambas, 2015; Koftis et al., 2015; Kokkinos et al., 2014).

Moving closer to numerical modelling of coastal flood components discussed above, Chini and Stansby (2012) presented a modelling system for determining wave overtopping discharge depending on water level and nearshore wave height. Kokkinos et al. (2014) assessed wave run-up and storm surge in the Aegean Sea using large wave data characteristics proving the vulnerability to flooding for the examined coastal areas. Gallien et al. (2014) took advantage of flood field observations in order to evaluate the accuracy of two urban flood prediction models. The first one, termed static, compares water level to land elevation while the second one, and more sophisticated, is based on a hydrodynamic model using time-dependent overtopping rates and estimating the overland flow.

The issue of flood risk management in coastal regions has been on the research agendas of several national and EU funded projects (Oumeraci et al., 2015; RISC-KIT, 2015). The present research, undertaken within the framework of the project PEARL (Preparing for Extreme And Rare events in coastaL regions) is funded under the 7th Framework Programme for Research of the European Union (FP7/2007-2013). The main goal of PEARL is to develop adaptive, socio-technical risk management measures and strategies for coastal communities against extreme hydro-meteorological events minimizing social, economic and environmental impacts and increasing the resilience of coastal regions in Europe (Makropoulos et al., 2014, 2015).

The approach presented in this paper is an integrated methodology for long-term prediction of climate changes and their respective impacts on coastal zones, starting from the wind climate change ending with the calculation of wave overtopping and run-up. This is achieved by the combination and cooperation of various numerical models for predicting and simulating the related natural phenomena. The case study in which the proposed methodology is demonstrated is the coastal region of Rethymno in the island of Crete, Greece. The results can be used in future plans of local authorities in order to take appropriate measures to inform the residents and to support optimum design of future protection works. Due to the methodology's generic nature, it can be applied to any coastal region. Section 2 presents the complexities of the selected area of research (Rethymno) and introduces the framework of the methodology by specifying the chain of numerical models implemented. Section 3 highlights the main assumptions and the available data used for past and future projections of local wave climate data obtained for SWAN model (Booij et al., 1999; Ris et al., 1999), a third-generation wave model that computes random, short-crested, wind generated waves in open sea, coastal regions and inland waters. With offshore wave data available, definition and categorization of the storm events is accomplished in order to distinguish the severity of each event. Registered flood events in the port area of Rethymno, as reported by residents' testimonials, are categorized according to wind measurements conducted by the National Weather Service. This action verifies the storm characteristics arising from the suggested approach. The simulations are then fed, as boundary conditions, into a wave propagation model (Section 4) to simulate the wave characteristics and the hydrodynamic field nearshore (MIKE21 PMS, HD (DHI, 2007a,b,c)). Subsequently the characteristic wave height, as transformed through various physical processes (shoaling, refraction, breaking, etc.), is used to simulate wave run-up with an improved Boussinesq-type model MIKE21BW (DHI,

2007a,b,c), and to estimate the wave overtopping (EurOtop, 2007) in selected reaches along the coastal zone of Rethymno (Section 5). Section 6 discusses the methodology and presents the main conclusions, important results obtained and suggested areas for further investigation.

2. Methodology

2.1. Rethymno site description

The area under study (Fig. 1) is located at the Prefecture of Rethymno, which is one of the four Prefectures of Crete in Greece. Rethymno city's population stands at 32,468 inhabitants, which characterize it as the third most populous urban area in Crete. Rethymno is the centre of commercial, administrative and cultural activities of the homonymous Regional Unit where most of the human activities are being developed along the coastline of the harbour area. The area, where the methodology will be tested, includes the Port of Rethymno and the adjacent coastal area (a total area of about 14 km^2 with a coastline length of approximately 8 km).

Flooding has always been a serious problem for Rethymno. Major flood events have been encountered throughout the years, resulting in serious damages mainly in the Old Town of Rethymno and the east low-lying areas (Figs. 2—5). Furthermore, changes in wind conditions — potentially due to climatic changes — have resulted in more frequent occurrence of storm events. Extreme weather conditions of strong winds resulting in the creation of storm waves are combined sometimes with flash floods from ephemeral streams. Dire consequence of the extreme waves formulation were the violent wave overtopping along the windward breakwaters of the harbour, as shown in Fig. 5, threatening the stability of breakwaters and port facilities as well as the safety of human population. An additional severe result of wave overtopping is the flood inundation of the harbour's surface area and the surrounding roads. The quantities of seawater (see figure) that penetrates from the west (Parking area) during those storm events, overflows the harbour's surface area, as well as the wider coastal area, causing disruption to loading and unloading operations, damage to the port facilities and the cargo, traffic problems and damage to coastal shops and restaurants. The adjacent recreational beaches are also exposed to erosion, spoiling the coastal site and affecting the tourism's contribution to local economy.

The combined occurrence of extreme hydro-meteorological events poses a real threat to Rethymno's community and emphasizes the need for specific actionable roadmaps that will enhance the existing infrastructure and operational strategies against the danger of flood by helping stakeholders to identify areas that are sensitive to floods and also to define efficient flood management strategies including engineering, environmental and socio-economic measures for Rethymno.

2.2. Description of methodology followed and numerical models chain

The SWAN model is initially used to simulate the offshore wave characteristics (directional spectrum) taking into account the changes of wind climate, followed by the MIKE21 PMS model which is applied for the transformation of the offshore information to shallower regions, up to the coast. Finally, a combination of MIKE21 BW, EurOtop and empirical formulas are utilized for the computation of wave overtopping

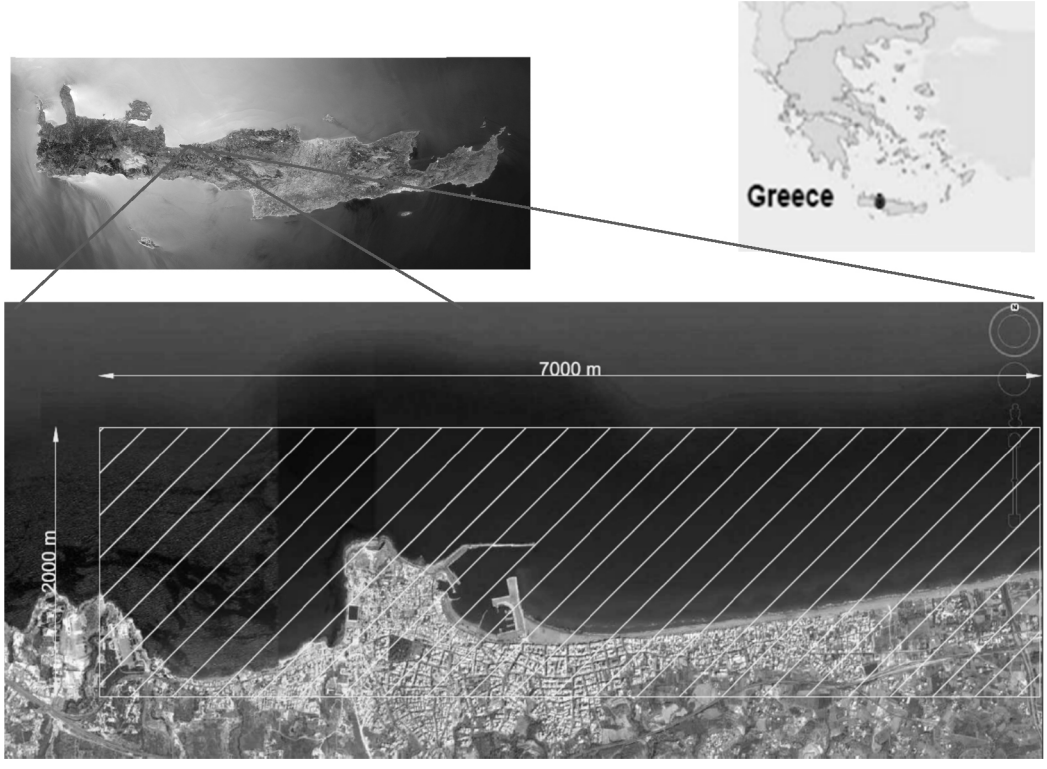

Figure 1 Rethymno city, Crete, Greece and area of interest.

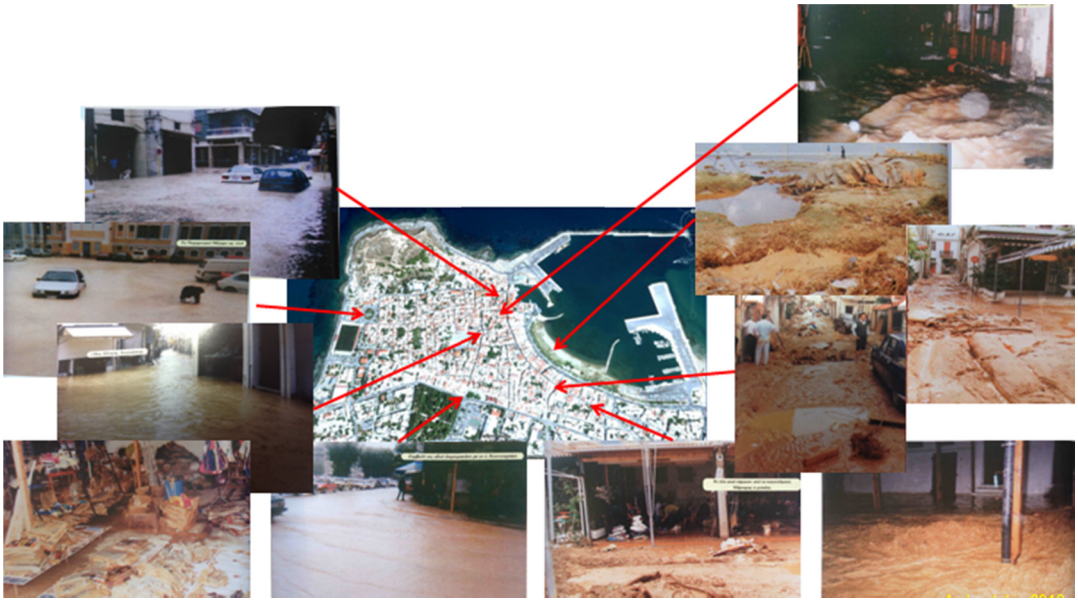

Figure 2 Historic flood in Rethymno, October 28th 1991 (Archontakis, 2013).

and run-up. The necessary wave condition at the offshore boundary of the local geographical area were derived from a downscaling approach, based on the transformation of global wind fields carrying the effect of climate change and affecting nearshore wave conditions. The latter are subsequently exploited for calculating the changes of wave overtopping and run-up which ultimately causes inland flooding of the coastal region of Rethymno's area.

The offshore wave simulations utilize a 3-level SWAN-based scheme (Athanassoulis et al., 2014) illustrated in

Figure 3 Recent floods at the harbour area of Rethymno (2010—2013).

Figure 4 Damages of the base of windward wave breakwater: (a) previous damages, photograph taken on January 4th, 2014; (b) new damages after structural repairs, photograph taken on January 14th, 2015.

Figure 5 Penetration of seawater through overtopping to the wider area of port facilities and debris from the windward wave breakwater damages.

Fig. 6 which was developed in the framework of Thales project CCSEAWAVS (Prinos, 2014) which aimed to estimate the effects of climate change on sea level and wave climate of the Greek seas, the coastal vulnerability and the safety of coastal and marine structures. This simulation scheme uses past and future projections climatic wind fields (also produced in the context of CCSEAWAVS) for the estimation of wave characteristics with resolution 0.2 × 0.2 degrees in the Mediterranean basin (Level 1). These data provide boundary information for repeating the simulation using a finer mesh 0.05 × 0.05 degrees inside an Eastern Mediterranean subsection (Level 2); see Fig. 6. Then, a high-resolution 0.005 × 0.005 degrees mesh is applied in the frames of the present work in the selected coastal region (Level 3). Details of the methodology are described in Athanassoulis et al. (2015). For evaluation purposes, systematic comparisons with results from the operational WAM-Cycle 4 implementation (courtesy of the Atmospheric Modelling & Weather Forecasting Group, University of Athens) were performed.

Within the present work, the Level 3 results of the offshore wave height, period, and direction are used to distinguish the usual incident waves from the storm surges. This is a

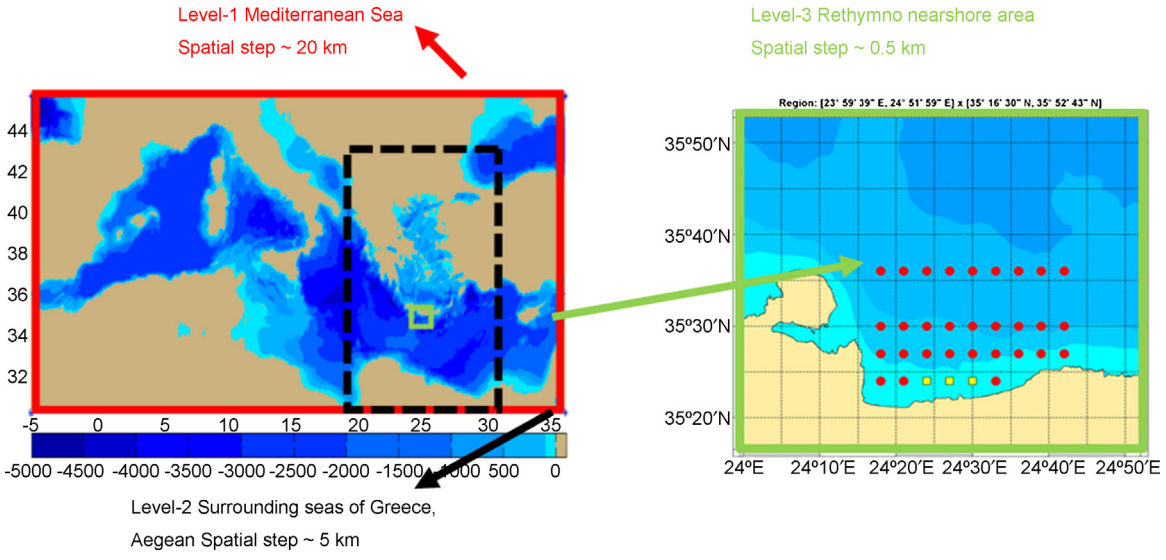

Figure 6 Estimation of offshore wave characteristics using a 3-level downscaling approach.

crucial step of the whole procedure, since the goal of this paper is to predict the extreme values of wave characteristics. The basic idea is to group storms into classes based on similar characteristics in order to apply the desired simulations for each category. Additionally, this will become valuable information for a future research dealing with the evaluation of coastal vulnerability for each class. Thus, many scientists of coastal study have made efforts to this direction. According to Dean and Dalrymple (2004) the destructiveness of a storm surge depends inter alia on its magnitude and duration and the wind-driven waves. Several attempts have been made after the Saffir-Simpson Scale (Saffir, 1977; Simpson, 1979) for storm intensity in the United States where hurricanes are placed in five classes depending on their central pressure, the maximum wind speed and the surge elevation. Halsey (1986) proposed a classification of Atlantic coast extratropical storms based on damage potential index. Dolan and Davis (1992, 1994) developed a classification of extratropical storms, or northeasters for the middle Atlantic coast, where an index of storm power was based on wave height and storm duration. They grouped and ranked the storms into five classes from weak to extreme, analogous to the Saffir—Simpson scale, using an average linkage clustering method. Concerning recent studies in Mediterranean Sea, Mendoza and Jiménez (2006, 2009) and Mendoza et al. (2011) provided a storm classification based on the beach erosion potential in Catalonian Coast and later for the Yucatan Peninsula (Mendoza et al., 2013) taking into consideration the storm energy and using the cluster analysis. The classification adopted here, is one of the most well-documented and it is based on the concept of the energy content (Dolan and Davis, 1992, 1994).

The above results are further exploited as boundary conditions for a coastal region phase-resolving simulation including the Rethymno area by means of a numerical wave model, based on the Parabolic Mild Slope equations (PMS, MIKE21). In this way the offshore wave characteristics are further downscaled in Level 4 taking into account additional local phenomena such as shoaling, refraction, bottom friction and wave breaking that take place in shallower water regions. The latter phenomena are well represented in the fine spatio-temporal mesh of Level 4 (as shown in Section 4, Fig. 16). The output of the above calculation provides subsequently the input to the hydrodynamic module through which the wave-induced current in the near shore area is calculated.

Ultimate step within Level 4 is the implementation of the empirical formulas and the MIKE21 BW wave model, so that computation of wave overtopping and run-up shall be achieved across the coastline. The latter model solves the so-called Boussinesq type equations in the time domain. It also resolves the wave propagation in detail and is best suited for simulation of nonlinear wave interactions, capable of reproducing the wave transformation across an arbitrary profile from intermediate waters up to the shoreline for the study of surf zone and swash zone dynamics. Herein, the 1D version is used to simulate the combination of setup and run-up whereas the empirical formulas are called for comparison. Additionally EurOtop, a widely accepted tool, is utilized incorporating techniques to investigate flood risk and predict wave overtopping at seawalls, breakwaters and other shoreline structures. This approach including the numerical chain is proposed in the present paper and the chart in Fig. 7 summarizes the above procedure in four discrete steps.

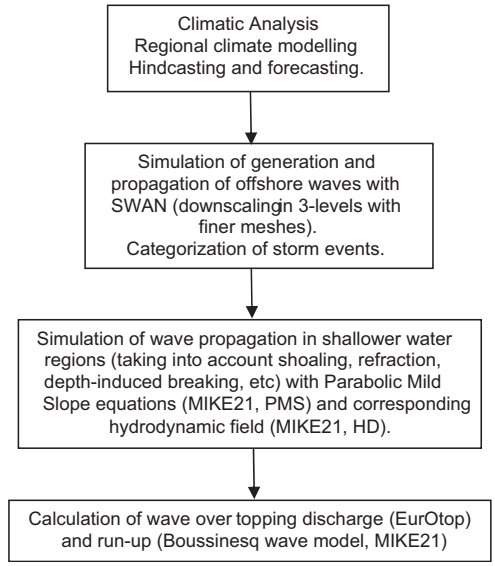

Figure 7 Flow chart depicting the proposed procedure.

Chini and Stansby (2012), as mentioned in Section 1, presented a similar downscaling procedure for determining wave overtopping depending on water level and nearshore wave height from global climate modelling. From offshore conditions to nearshore, waves were simulated using WAM (WAMDI-Group, 1988) and surges were modelled with the continental shelf tide and surge model CS3 (Williams and Flather, 2004). The nearshore wave propagation was achieved by using the third generation wave spectral model TOMAWAC, solving for the conservation of wave action on an unstructured mesh using the finite element method (Benoit et al., 1996). Finally, a neural network approach was used from EurOtop to calculate the overtopping discharge at a specific example of a vertical wall. The present approach provides a more integrated approach, providing results for both wave run-up and overtopping.

3. Projections of past and future wave climate (SWAN)

3.1. Atmospheric variables and climate change scenario

The wind data used as forcing of the SWAN simulation over Rethymno were also one of the outcomes of the CCSEAWAVS project (Velikou et al., 2014). Over the northeast Atlantic and Europe, the regional atmospheric model REMO, which is based on the Europamodel/Deutschland model system (Majewski and Schrodin, 1994), was used in order to get a high resolution atmospheric forcing. Climatic analysis of the Mediterranean and the Greek sea area and eventually estimation of atmospheric variables was achieved by utilizing the RegCM regional model (RegCNET: regional climate network, 2003). Its spatial analysis is 25 km $\times$ 25 km and for the future projections of atmospheric (10 m wind, atmospheric pressure, air temperature) data the model is using the AR4-A1B emission scenario. Past projections for 1960—2000 are based on input from measured carbon dioxide emissions. Enhanced

simulated data in the Greek Sea region have also been derived from the new version of RegCM3_10 regional model, with 10 km × 10 km spatial resolution (Velikou et al., 2014). RegCM3_25 model uses 18 vertical levels on a horizontal 192 × 108 grid and a time step of 60 s. RegCM3_10 model is nested inside the RegCM3_25 model and uses 18 vertical levels on a horizontal 128 × 160 grid and a time step of 30 s.

3.2. Study area, bathymetry and computational grid

The Level 3 SWAN simulation was performed in a rectangular frame with limits 35.3E, 35.7E Latitude and 24.25N, 24.75N Longitude. With a regular resolution of 0.005 × 0.005 degrees for Level 3, the produced computational grid consists of 8181 grid points of which 6471 are wet-points and the rest fall on land. The bathymetry was obtained from the combination of the General Bathymetric Chart of the Oceans database (GEBCO, 2009) and a nautical chart from the Hellenic Navy Hydrographic Service. In particular, the GEBCO database was used for depths higher than 500 m and digitized nautical chart contours for depths lower or equal to 500 m, along with the digitized coastline (Fig. 8).

The distribution of significant wave height, wave peak period and mean wave direction at points n depicted in Fig. 8, for one past (1961–2000) and two bi-centurial future periods (2001–2050, 2051–2100) is shown in Fig. 9. In general, the projected future distributions remain very close to those of the past period. Some weak but noticeable variations are observed during period 2051–2100, with higher occurrence of waves originating from the North sector. Although relatively small, this probability shift towards southward waves can be significant due to the North-facing orientation of Rethymno coast.

The seasonal pattern (mean value for each month) for the same time-periods is illustrated in Fig. 10. The seasonal pattern is similar for the two parameters, which is expected due to the high correlation between wave height and wave period. Mean values for period 2051–2100 are generally equal or higher to that of the other two periods with the exception of 3 months (October–December). The higher mean value during the last period is also noticeable in

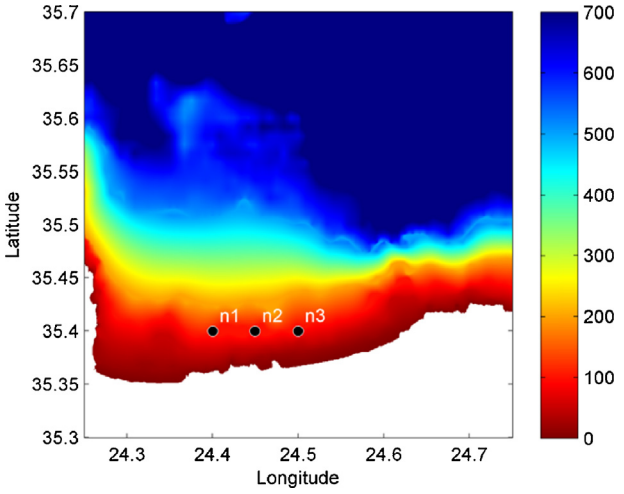

Figure 8 Bathymetric map used for Level 3 simulation.

Fig. 9, where a small reduction of the distribution peak is observed for both the significant wave height and peak period, implying an increased mean value due to the log-normal probability form.

3.3. Categorization of storm surge events, joint probability of significant wave height and period, sea level rise

With offshore wave data available, a definition and categorization of storm events can be derived, in order to treat the storm surges in group and not individually and to link them with respective factors of coastal vulnerability in a future research. This is done by following the definition and identification of the storms through the energy content as proposed by Dolan and Davis (1992). The classification is accomplished into five classes: I – weak, II – moderate, III – significant, IV – severe and V – extreme. The first step before applying this approach is the characterization of the forcing. A storm is defined as the event exceeding a minimum significant wave height (e.g. $H_s > 2$ m) and with a minimum duration of 6 h (Li et al., 2014; Michele et al., 2007). The

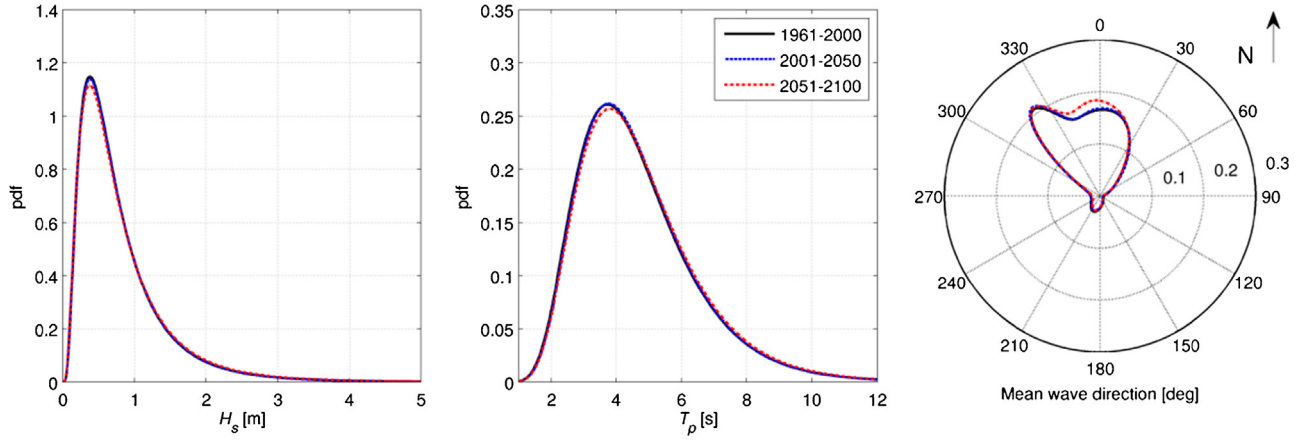

Figure 9 Probability density functions for the significant wave height H_s (left panel), peak wave period T_p (central panel) and mean wave direction (right panel), for three time periods, at points n*i* (*i* = 1–3) (shown in Fig. 8).

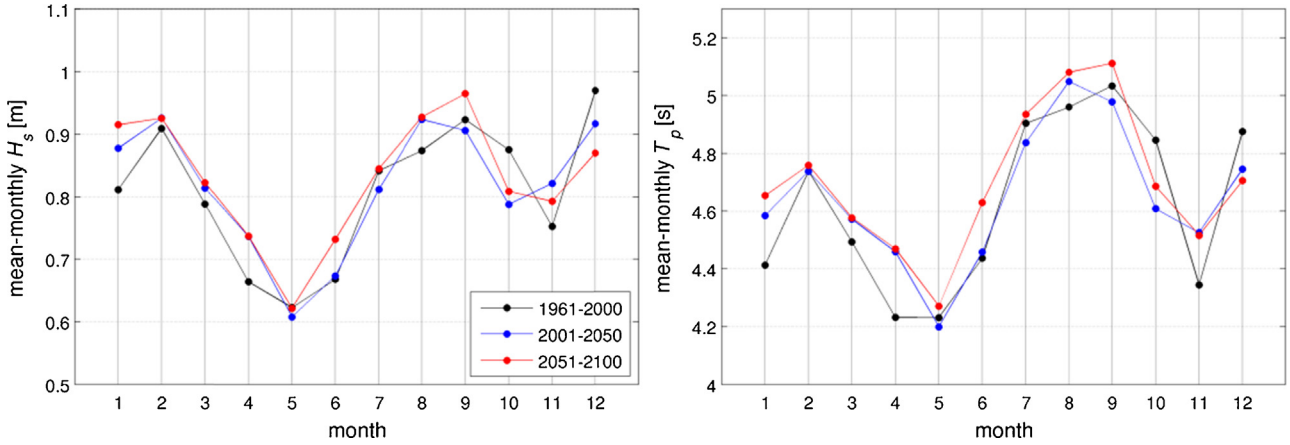

Figure 10 Seasonal pattern of the significant wave height H_s (left panel) and peak wave period (right panel) T_p for three time periods, at points n*i* (i = 1–3) (shown in Fig. 8).

threshold of significant wave height (H_s) is considered to be 2 m in order to describe rare events with only 10% of total wave heights and thus defined as the 90th percentile of the data set (Rangel-Buitrago and Anfuso, 2011). The energy content of each event is then calculated as follows:

$$E = \int_{t_1}^{t_2} H_s^2 \, dt, \tag{1}$$

where (t_1–t_2) is the storm duration and H_s is always greater than H_s threshold.

The above analysis has been divided into two periods: 1960–2000 (past climate) and 2000–2100 (future climate). It has to be noted here that this technique has also been applied by other researchers in regions close to Rethymno (e.g. Chania, Crete Island, Kokkinos et al., 2014). The analysis is done for the North wind direction since it is the dominant one that generates incident waves to the Rethymno coast.

The results of the average wave height, period and duration in n2 grid point, in Fig. 8, for each storm class are given in the following Tables 1 and 2 for the North wind direction and in Tables 3 and 4 for the Northwest wind direction. The extracted results came from n2 and n1 grid points, of Fig. 8, respectively for the two incident directions. Although the result of SWAN program gives an accuracy of 7 decimals for both variables, an accuracy of 1 decimal was selected herein, since it is answered in many engineering applications as well.

Inspection of the below provided results presents that the range of the wave height lies between 2 m (which is the minimum value that has been determined in this paper in order to have a storm event) up to almost 6 m. The specific range appears the same in any storm class which can be attributed to the fact that a storm event can consist of a sequence of small wave heights e.g. 2 or 3 m for long time

Table 1 Storm events for the period 1960–2000 N direction.

North wind direction 1960–2000							
Storm class		H_s range [m]	T_p range [s]	Average H_s [m]	Average T_p [s]	Average duration [h]	No. of events
I	Weak	2.0–4.6	6.2–9.4	2.5	7.7	14.20	318
II	Moderate	2.0–5.7	6.5–10.0	2.9	8.1	34.50	27
III	Significant	2.0–4.6	7.5–9.6	3.6	8.1	44.25	4
IV	Severe	2.0–5.6	6.7–10.7	3.3	8.3	72.50	6
V	Extreme	–	–	–	–	–	0

Table 2 Storm events for the period 2000–2100 N direction.

North wind direction 2000–2100							
Storm class		H_s range [m]	T_p range [s]	Average H_s [m]	Average T_p [s]	Average duration [h]	No. of events
I	Weak	2.0–5.3	6.4–10.1	2.5	7.7	14.13	823
II	Moderate	2.0–5.0	6.7–9.9	2.7	8.0	42.03	94
III	Significant	2.0–6.0	6.9–10.3	3.0	8.2	61.84	13
IV	Severe	2.0–5.4	6.4–10.0	3.2	8.2	81.38	8
V	Extreme	2.0–5.0	7.8–9.7	4.2	9.1	72.00	1

Table 3 Storm events for the period 1960–2000 NW direction.

Northwest wind direction 1960–2000							
Storm class		H_s range [m]	T_p range [s]	Average H_s [m]	Average T_p [s]	Average duration [h]	No. of events
I	Weak	2.5–4.6	6.2–9.4	2.5	7.7	11.40	10

Table 4 Storm events for the period 2000–2100 NW direction.

North wind direction 2000–2100							
Storm class		H_s range [m]	T_p range [s]	Average H_s [m]	Average T_p [s]	Average duration [h]	No. of events
I	Weak	2–4.6	6.2–9.4	2.5	7.7	10.55	33
II	Moderate	2–5.7	6.5–10.0	3.0	8.1	39.00	1

duration or in a sequence of large wave heights for a small duration. Besides, during the evolution of every storm event, small or large wave heights can appear. Obviously, by climbing storm class there is a tendency of the average wave heights and periods to be increased. As could be observed in Table 1 the upper limits of H_s and T_p ranges are greater in class IV in comparison with class III. The average values though remain smaller. This can be attributed to the small population of storm events for both categories.

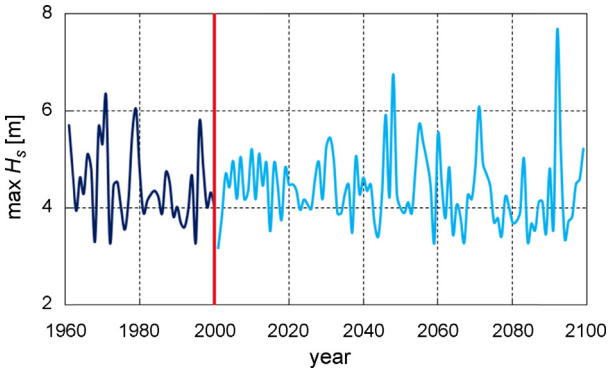

Figure 11 Maximum wave height (max H_s) per year for the two periods (1960–2000, blue line and 2000–2100, light blue line). (For interpretation of the references to colour in this figure legend, the reader is referred to the web version of this article.)

In order to gain a more integrated view of the future wave climate in the offshore region of Rethymno, the maximum wave height (max H_s) per year for the two periods is also depicted in Fig. 11 as obtained by the wave data in n2 grid point. One can observe that the maximum wave height is close to 8 m. However, this value appears in different wind direction than the North one which is of the greatest interest in the present paper. The maximum wave height coming from North was calculated at 5.95 m as presented in the above table.

Additionally the joint distributions of significant wave height H_s and peak wave period T_p at n2 grid point of Fig. 8, normalized to the respective average values of them (H_m and T_m) are given for the two examined different periods: 1960–2000 in Fig. 12 and 2000–2100 in Fig. 13 respectively. It is observed, through the high values of the corresponding correlation factor $r(H_s, T_p)$ that these two wave parameters are well correlated for extreme wave

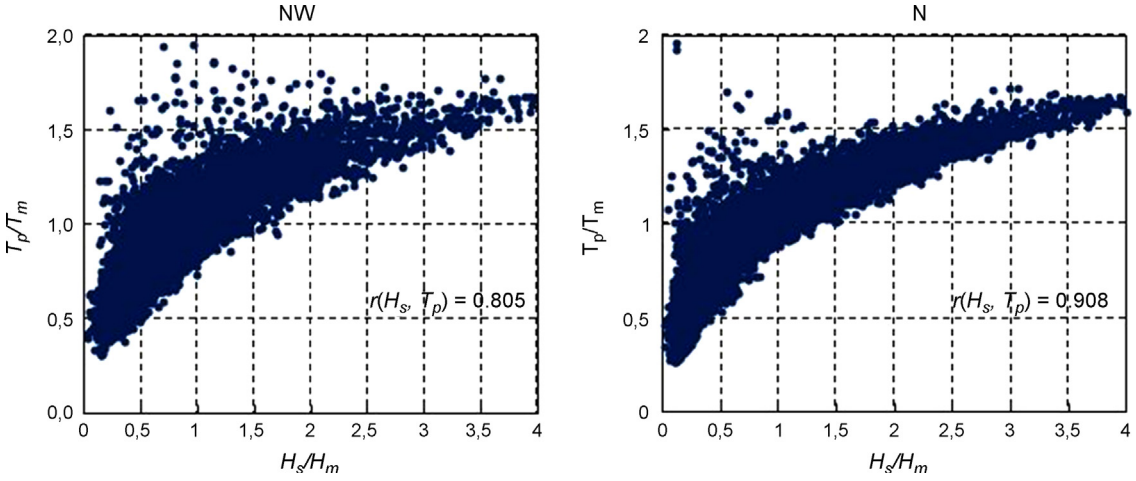

Figure 12 Scatter plots of normalized significant wave heights (H_s/H_m) and peak periods (T_p/T_m) for period 1960–2000 and for NW and N wind directions.

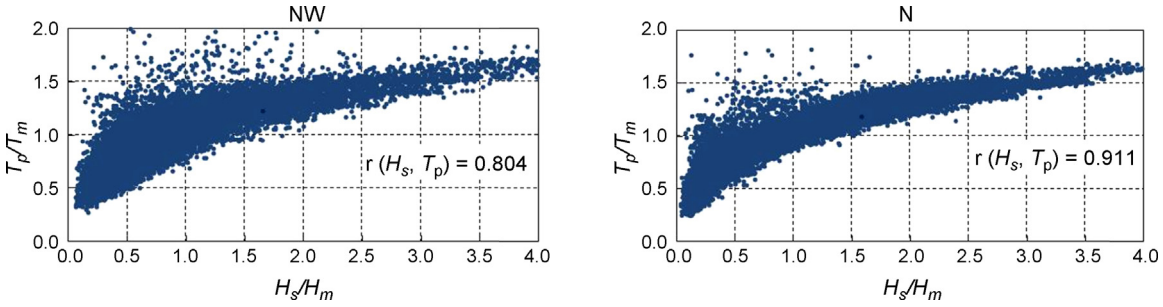

Figure 13 Scatter plots of normalized significant wave heights (H_s/H_m) and peak periods (T_p/T_m) for period 2000–2100 and for NW and N wind directions.

heights. Full dependence between extreme significant wave height and peak wave period is therefore assumed.

3.4. Observed storm surge and flood events

Recorded historical wave overtopping events (Galanis, 2010) include events that developed mainly in the port area, whose respective dates are presented in Table 5.

In order to distinguish the class of each of the above storm events the following procedure is applied. Firstly, the fetch effective F_{eff}, is calculated through CEM (2008) for the two dominant directions of wind i.e. North and Northwest, yielding to 281.8 km and 224.5 km respectively. The next step takes advantage of the continuous measurements of wind velocity and wind direction in the area of Rethymno every 3 h by the National Weather Service. These field measurements hold from 1958 up to date. However, the manageable data is limited until the year 2008. Thus, only the first three events of Table 5 can be categorized. In Figs. 14–16 the measured wind characteristics are illustrated.

The mean values of the above events are summarized in Table 6. It has to be mentioned that 360° denote the north wind direction, hence the first case is included to the northwest direction while the rest in the north.

Finally, having in mind the F_{eff} and the wind speed, along with the respective duration, the developed characteristic of wave e.g. wave height H_s and peak wave period T_p were calculated using the SMB wave prediction method (Bretschneider, 1952, 1958). Each storm event is then classified by applying Eq. (1). The results are given in Table 7.

As it is observed, the reported storm events are up to the third (III) class for north wind direction and to the first (I) for the northwest, proving that the above classification respond satisfactorily to reality. However, the storm class that derived herein are five (Table 1) and two respectively (Table 3) for the two directions, but it should be kept in mind that the above flood events, reported from the residents, are limited and indisputably cannot capture all the events that took place.

Table 5 Dates of flood events in the port area of Rethymno.

No.	Date	Year
1	20/11–21/11	1964
2	05/10–07/10	1989
3	28/11–29/11	2000
4	11/12	2010
5	28/02	2012
6	03/12	2013
7	11/12	2013

4. Numerical simulation of wave and hydrodynamic field

The bathymetry of Rethymno coastal area is constructed into a grid (Fig. 17) with dimensions 5.5 km × 6.2 km in x and y axes respectively. The spatial step is chosen $dx = dy = 5$ m. The bathymetry has been rotated counter clockwise at 90° due to requirements of MIKE21 PMS.

The average values of wave height and period of each storm class are adopted as input data and numerical simulations with MIKE21 PMS are carried out to estimate the spatial evolution of these quantities in the whole coastal area. Consequently, the resulting radiation stresses serve as input to the hydrodynamic module with MIKE21 HD to investigate the spatial evolution of the velocity. The results are depicted in Figs. 18 and 19 for the spatial distribution of significant wave height and in Figs. 20 and 21, for the hydrodynamic field for the total of five storm categories (I–V) in case of north wind direction and for the two storm categories in case of northwest wind direction (I, II). Furthermore, simulations have been carried out for the maximum incident wave as derived by the above analysis. The wave height of it equals to $H_s = 6.0$ m and the peak period is $T_p = 10$ s. These results are also presented in Figs. 18 and 20 for the spatial distribution of significant wave height and the hydrodynamic field respectively.

As it is obvious, from the above figures, one can notice the effect of refraction, as waves approaching the shallower region and the mean wave direction (represented by arrows) tend to be perpendicular to the coastline. Furthermore, diffraction phenomenon is satisfactorily simulated inside the port basin (denoted e.g. by red circle in the bottom, Fig. 20) providing the respective wave disturbance in that area for each storm class intensity. The coloured contours give information for the spatial evolution of wave height and for the breaking line that moves away from the shoreline as the storm class increase since the incident wave height increase as well. In any scenario of the above eight (for each storm class – including the maximum occurred incident wave $H_s = 6.0$ m and for each direction), the magnitude of wave

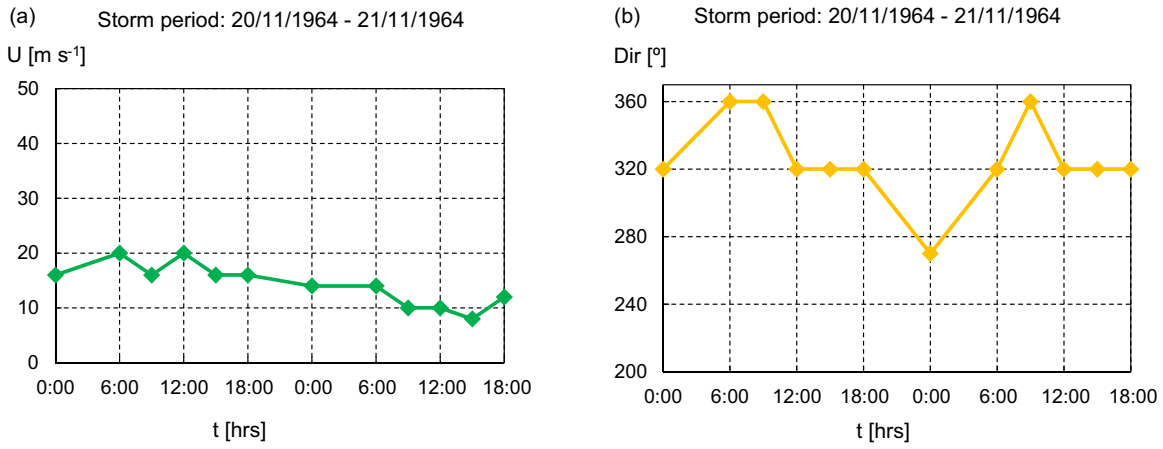

Figure 14 Wind characteristics: (a) wind velocity and (b) wind direction for Case No. 1 of Table 5.

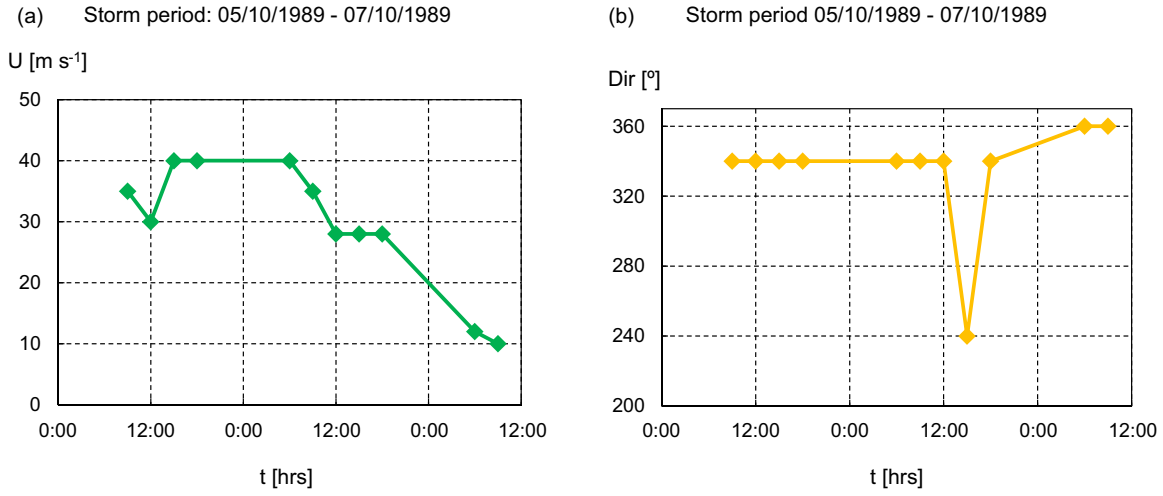

Figure 15 Wind characteristics: (a) wind velocity and (b) wind direction for Case No. 2 of Table 5.

heights in the area of the windward breakwater of the port is significantly greater than the respective approaching the shoreline. This was expected since the energy dissipation from depth-induced breaking in the first case is smaller than the second one. It will be shown in the next section that information about the wave height in this area, calculated by PMS, is essential for the proper calculation of overtopping.

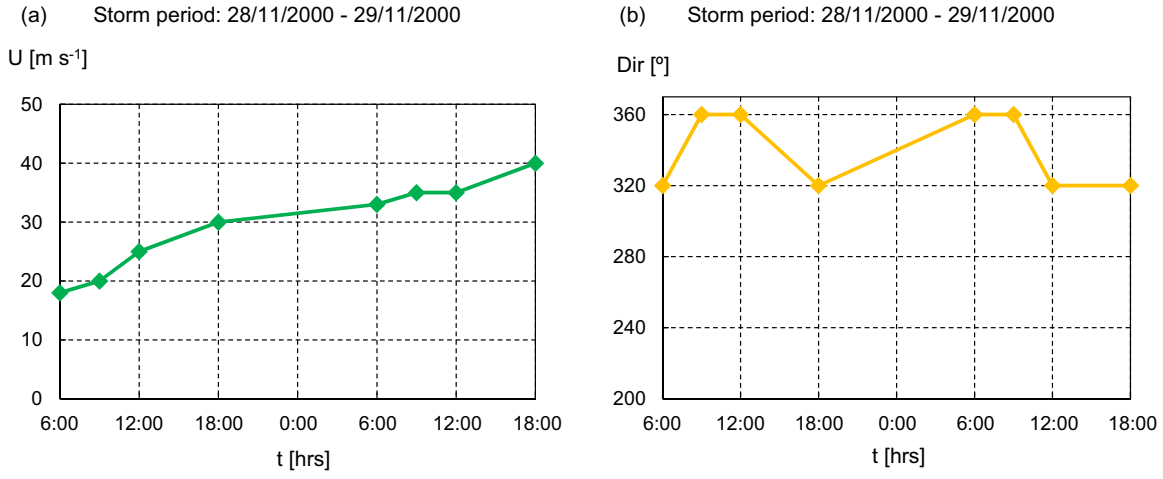

Figure 16 Wind characteristics: (a) wind velocity and (b) wind direction for Case No. 3 of Table 5.

Table 6 Mean characteristics of storm events as extracted by field measurements.

No.	Year	Wind velocity [m s^{-1}]	Wind direction [°]	Duration [h]
1	1964	7.4	326	42
2	1989	15.3	335	48
3	2000	15.2	340	36

Table 7 Classification of storm events by field measurements.

No.	Wind direction	H_s [m]	T_p [s]	Storm class
1	NW	1.6	6.6	I
2	N	3.8	7.8	III
3	N	3.8	7.8	II

As the storm intensity increases, the wave heights increase in the whole domain, generating strongest currents. The basic conclusion of the above figures depicting the hydrodynamic field, lies on the illustration of the most vulnerable sub areas where the magnitude of velocity components increase. Thus, in the sub area of the port and the area west of it, (denoted e.g. by red circles in the bottom above, Fig. 20) strongest movement of the currents are observed. This is in accordance with the physical observations where the most flood events are taking place in the respective locations of Rethymno as shown in Figs. 2—5. Another interesting point, that was expected and it is well simulated by the hydrodynamic model, is the generation of more dominant long-shore currents in the case of northwest direction, since the oblique wave incidence lead to greater values of radiation stresses (denoted e.g. by red circle in the right of Fig. 21). Unfortunately, these valuable results of the hydrodynamic field certainly affecting run-up and overtopping cannot be incorporated in the majority of numerical models, capable of predicting these processes, as boundary conditions, especially in one horizontal dimension models. Nonetheless, the simulation of spatial evolution of current velocities in one hand give a more integrated picture of the physical processes taking part in

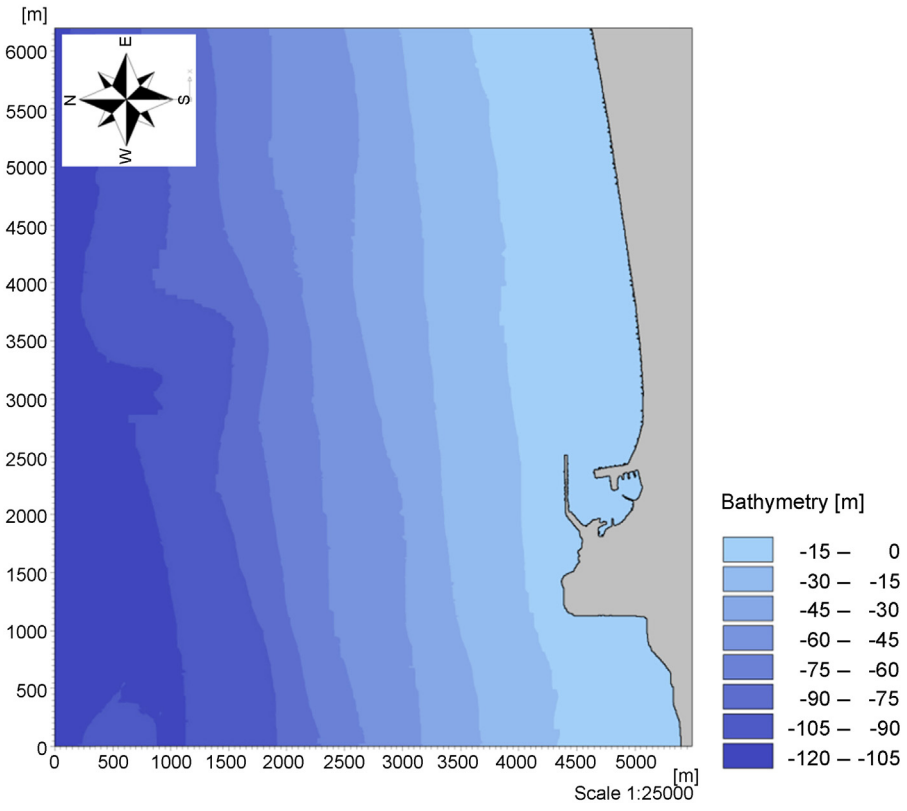

Figure 17 Numerical grid of Rethymno's bathymetry.

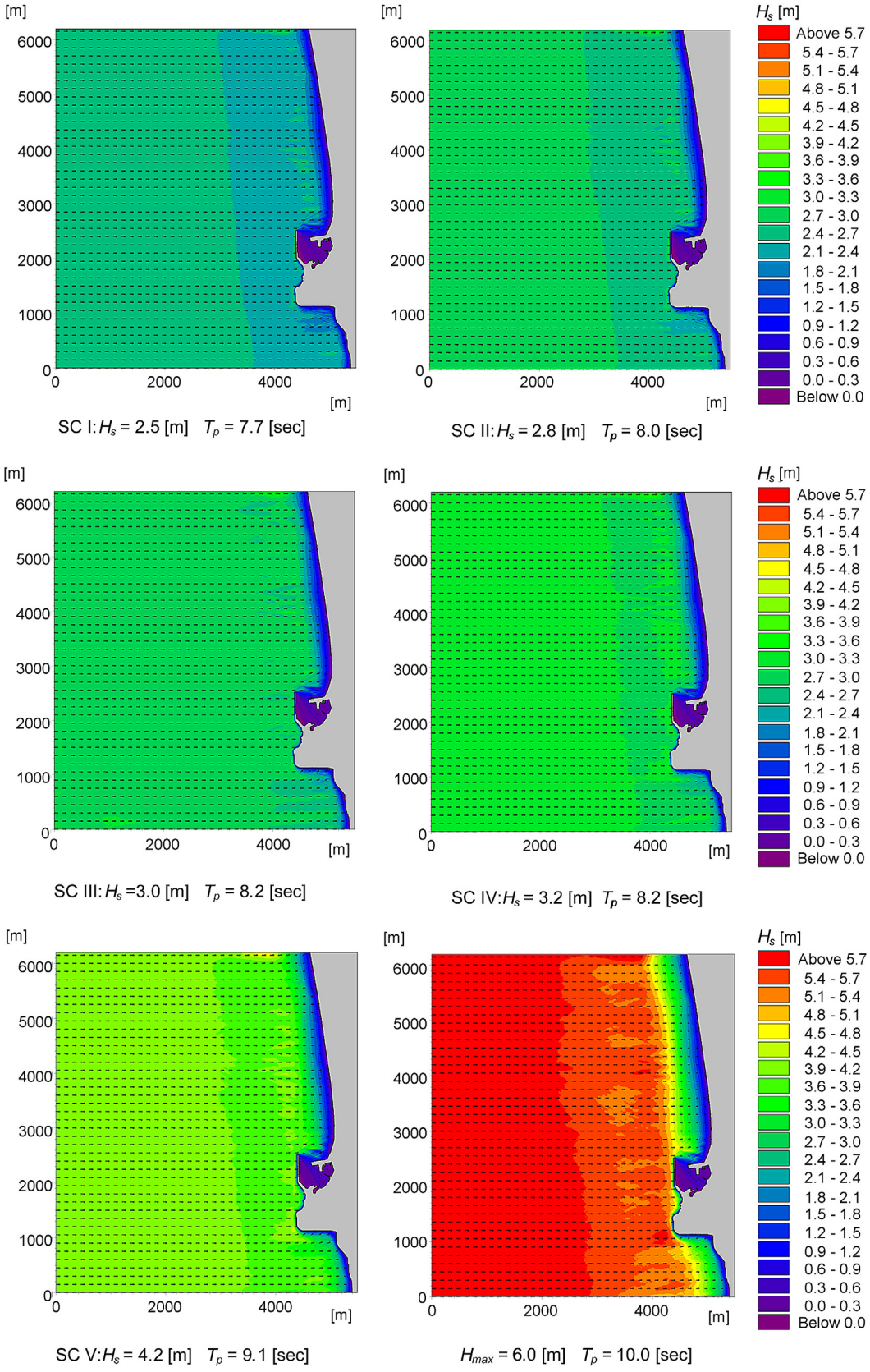

Figure 18 Spatial distribution of significant wave height (H_s) for storm classes (SC) I to V and for the maximum occurred incident wave H_{max} = 6.0 m for the north direction. Arrows denote the mean wave direction. The colour legend of wave height contours is identical for all classes.

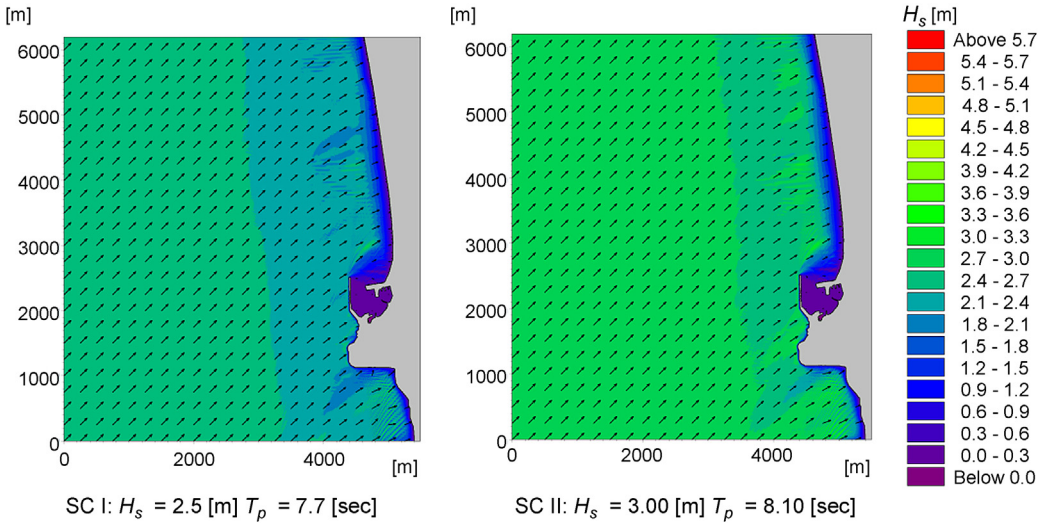

Figure 19 Spatial distribution of significant wave height (H_s) for storm classes (SC) I and II for the northwest direction. Arrows denote the mean wave direction.

the real field and cannot be avoided and on the other hand it is necessary for prediction of sediment transport in the area, which is a work on progress.

5. Wave overtopping and run-up

By taking advantage of the simulated wave propagation into shallower water regions and the corresponding nearshore wave characteristics, the wave overtopping and run-up can be estimated at any desired profile of the whole field under study.

5.1. Bathymetric profiles and chosen section

The wave run-up is calculated at two bathymetric profiles, arbitrarily chosen but representative of the mean profile of sea bottom in the area of interest, east and west of the port (Fig. 22) with a mean bottom slope equals to 3%. While the overtopping is calculated at section A-A′ of the port (Fig. 23) which is a characteristic section of the current port constructions, consisting of an upwind breakwater and a vertical quay wall in the leeside, it must be underlined that the proposed methodology can be proved really useful for redesigning future protection projects since the estimation of overtopping and run-up is available, with no extra time or computational cost.

5.2. Wave run-up

Wave run-up, *Ru* [m] is the extreme vertical height of the wave on a beach, and it is affected by the wave setup and swash. This quantity can be estimated through the following ways:

1. *Empirical formula as derived by* Stockdon et al. (2006)

$$Ru = 1.1 \times \left(0.35\tan\beta(H_s L_0)^{1/2} + \left(H_s L_0 \frac{(0.536\tan\beta^2 + 0.004)^{1/2}}{2}\right)\right), \quad (2)$$

where tan β is the beach slope and L_0 is the deep water wave length associated to the wave peak period T_p for each storm (all values are in m). The final *Ru* for each storm class is obtained by taking the average wave height calculated for all storms.

2. *Irregular wave run-up Equation of Coastal Engineering Manual* (CEM, 2008)

$$\frac{Ru}{H_s} = \begin{cases} 0.96\xi & \text{for } 1.0 < \xi < 1.5 \\ 1.17\xi^{0.46} & \text{for } 1.5 < \xi \end{cases}, \quad (3)$$

where ξ is the Irribaren number defined as: $\xi = \frac{\tan a}{\sqrt{H_s/L_0}}$.

3. *Numerical simulation with the 1D version of a Boussinesq-type wave model (MIKE21 BW).*

The wave characteristics (H_s, T_p), as calculated by PMS in intermediate water are fed into the time-dependant model as irregular time series of surface elevation along with the bathymetric profile. The recommended values (DHI, 2007a,b,c) are used in MKE21 BW for simulation of wave breaking and bottom friction.

The results for the five different storm classes for the three different approaches are given in Table 8. Inspection of the above results proves a deviation between the methods of run-up calculation for each storm class. In the present paper the latter method of numerical modelling is proposed, since it is based on a Boussinesq model simulating the time-dependent propagation of the wave train taking into account the changes in bathymetric profile and not just the bottom slope, thus, it is closer to real life sea state.

5.3. Wave overtopping

Calculation of mean overtopping discharge rate is the last step of the methodology, but of primary importance since it enables further estimation of the inland flooding due to storm events. By inserting wave characteristics i.g: wave height at the toe of the structure (H_{m0}) and wave period (T) and geometrical characteristics i.g: the height of the crest of the wall above still water (R_c); the width of the structure crest G_c; the coefficient for reduction factors (γ) depending

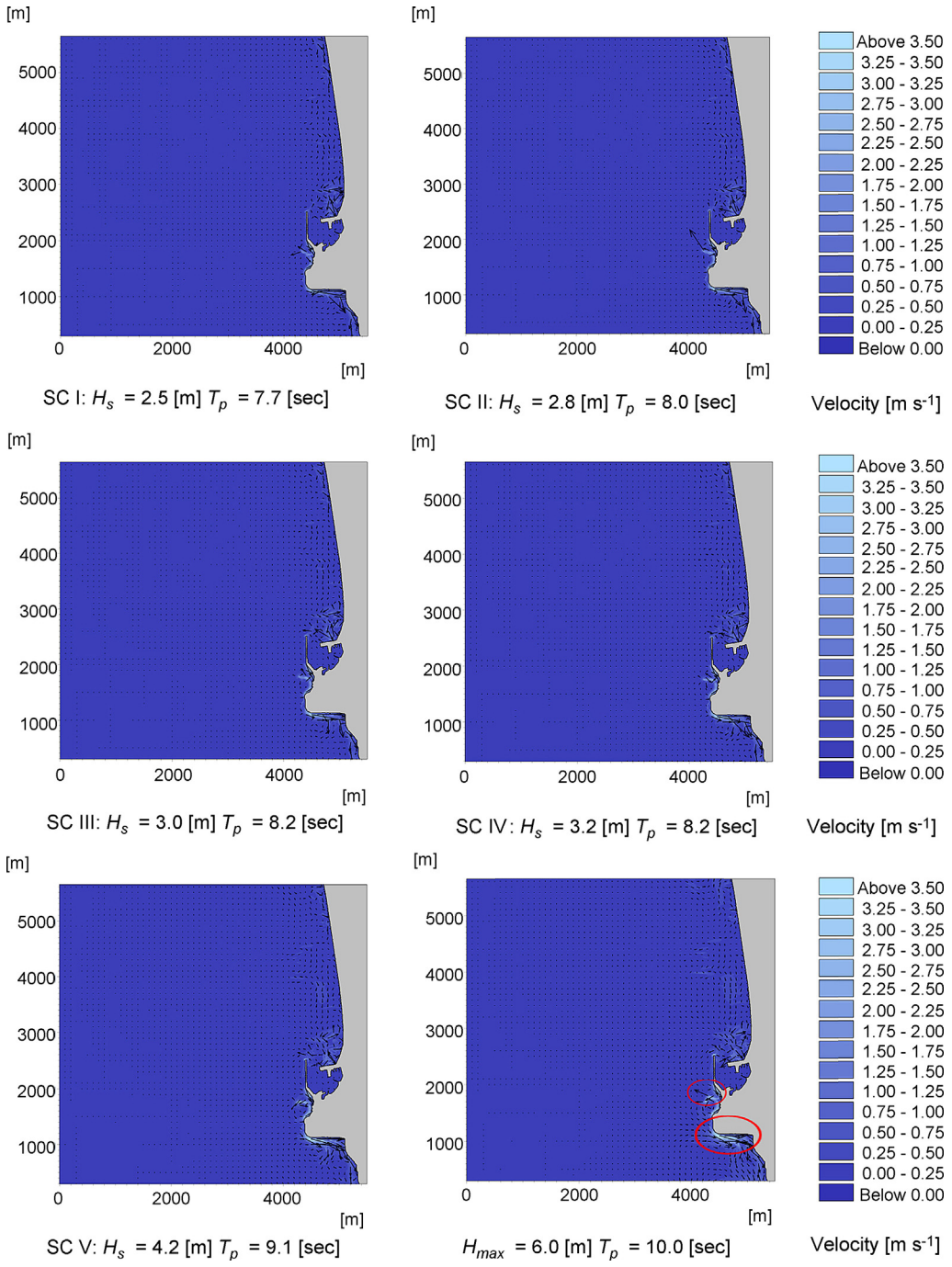

Figure 20 Hydrodynamic field for storm classes (SC) I to V and for the maximum occurred incident wave H_{max} = 6.0 m for the north direction. Arrows denote the current direction. The colour legend of wave height contours is identical for all classes.

on the permeability, into the EurOtop tools (EurOtop, 2007), such as parametric equations and artificial neural networks one can calculate the overtopping. The section A-A′ depicted in Fig. 22 is similar to the one of Fig. 24 and thus one can calculate the mean discharge rate per metre run of seawall Q [l s^{-1} m^{-1}] as shown in Table 9.

As it was expected, wave run-up and overtopping discharge increase as the intensity of the phenomenon increases. Nonetheless, the rapid increase of the overtopping for the extreme class (V) of the storm is worth of mentioning.

6. Discussion and conclusions

There is a growing interest in the development of reliable scenarios (future projections) for climate change affecting inter alia the frequency of storm surge events, the magnitude

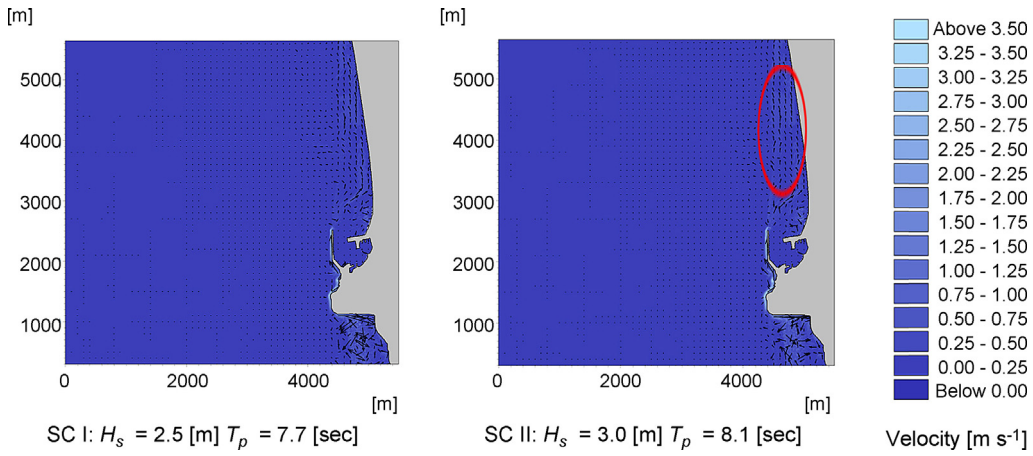

Figure 21 Hydrodynamic field for storm classes (SC) I and II for the northwest direction. Arrows denote the current direction.

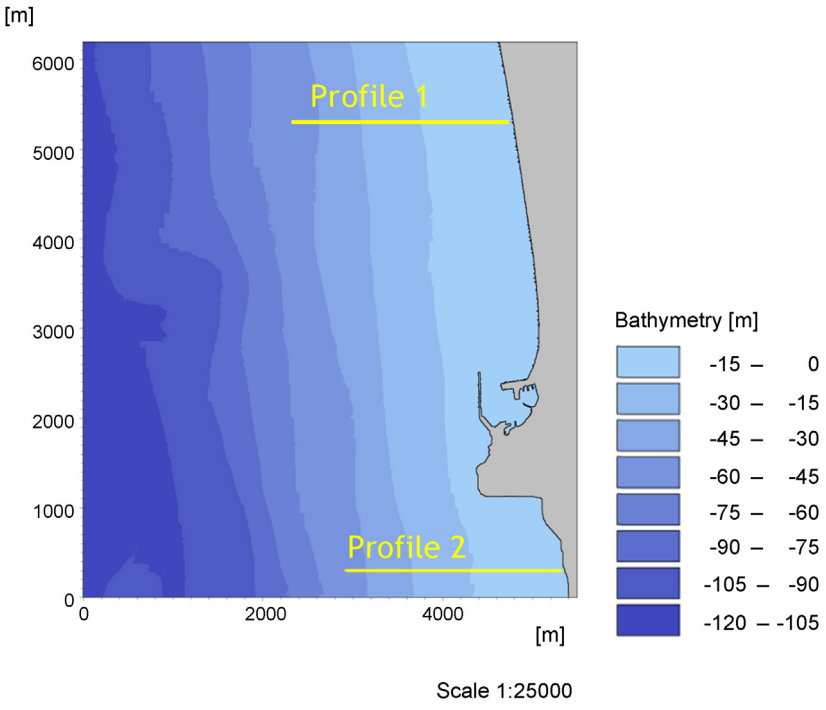

Figure 22 Selected bathymetric profiles for estimation of wave run-up.

Table 8 Calculation of wave run-up *Ru* [m] for the 2 different beach profiles of Fig. 22.

Storm class		*Ru* [m] for Profile 1			*Ru* [m] for Profile 2		
		Empirical Stockdon et al. (2006)	Empirical CEM (2006)	Numerical Boussinesq (MIKE21)	Empirical Stockdon et al. (2006)	Empirical CEM (2006)	Numerical Boussinesq (MIKE21)
I	Weak	0.84	1.14	0.57	0.84	1.14	0.67
II	Moderate	1.01	1.26	0.64	1.01	1.26	0.71
III	Significant	1.14	1.34	0.69	1.14	1.34	0.72
IV	Severe	1.24	1.42	0.7	1.24	1.42	0.75
V	Extreme	1.94	1.78	0.78	1.94	1.78	0.90

Figure 23 Selected cross section of the breakwater for estimation of wave overtopping.

Table 9 Mean overtopping discharge rate Q (Section A-A′).

Storm class	Input data					Output data
	H_{m0} [m]	T_p [s]	R_c [m]	G_c [m]	γ	Q [l s^{-1} m^{-1}]
I	2.33	7.68	6.1	4	0.55	0.002
II	2.64	7.99	6.1	4	0.55	0.015
III	2.85	8.19	6.1	4	0.55	0.045
IV	3.00	8.24	6.1	4	0.55	0.090
V	4.04	9.08	6.1	4	0.55	2.801

of wave heights, stronger currents and sea level rise. The above phenomena increase the flood risk for coastal areas and induce morphodynamic changes and as such their study is crucial for design and construction of climate resilient protection works.

In this paper, an integrated approach is proposed to calculate the wave overtopping and run-up through a chain of numerical tools starting from regional climate change models and ending nearshore. The first discrete step consists of climatic projections of wind forcing based on a potential emission scenario (e.g. AR4-A1B) and afterwards the simulation of offshore wave generation and propagation. It is expected that further emission scenarios will be selected and applied in the future to provide a more comprehensive picture of the future situation.

The proposed approach includes the categorization of storm events to avoid (i) individually handling of every event and (ii) to arrive at consolidated results. This was undertaken using an energy concept. Field data measurements of wind velocities and direction up to year 2008 were used to verify

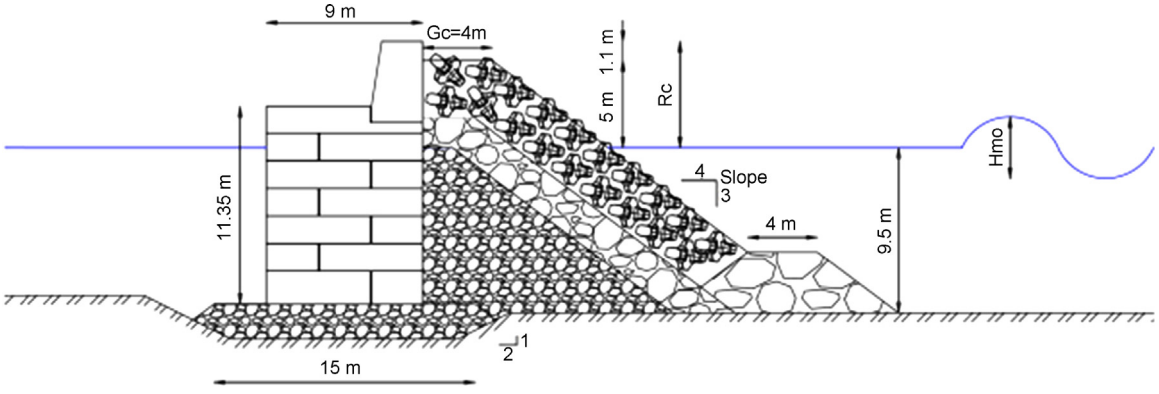

Figure 24 Definition sketch of breakwater cross section A-A′.

the outcomes of the model, showing a satisfactory correspondence concerning the classification of storm events. However, more reported storm events from 2008 up to date must be taken into consideration as soon as the relevant wind data are available from the National Weather Service.

The results of wave and hydrodynamic field simulations, by the means of a Parabolic Mild Slope model and a Hydrodynamic model, showed a good performance able to account for the spatial evolution of wave heights and velocity currents respectively. The modelled area, where wave breaking is more intense (on vertical fronts) and the generated currents become stronger, agrees fairly well with the field observations i.e. the port area of Rethymno, where the majority of coastal floods are reported. Finally, the implementation of Boussinesq model and EurOtop provides an advantage towards the accurate calculation of wave run up and overtopping respectively.

It can be argued that this procedure has a broader application range and can be adopted in any coastal region. The discrete steps, described in the methodology, can be adapted for any climate change scenario, bathymetry and topography of the potential coastal area of interest. We suggest that further research efforts should follow two main, interesting, directions: The first one would include the simulation of flooding within the urban areas by means of a hydrodynamic model, based on wave overtopping and run up results, and by taking into account current urban geometry (buildings, drainage, topography, etc.) but also possibly future urban form resulting from urban growth simulations (Bouziotas et al., 2015). The second direction is to embed the results into National and/or Local authorities planning policies, possibly using a collaborative knowledge co-production approach (Evers et al., 2012) to investigate options for flood risk management practices based on the calculated vulnerability of the coastal area.

References

Anselme, B., Durand, P., Thomas, Y.-F., Nicolae Lerma, A., 2011. Storm extreme levels and coastal flood hazards: a parametric approach on the French coast of Languedoc (district of Leucate). C. R. Geosci. 343 (10), 677—690, http://dx.doi.org/10.1016/j.crte.2011.07.006.

Archontakis, D., 2013. The Old Town of Rethymno: from a run down gheto to growth leverage of Rethymno. Rethymno, 12—18.

Athanassoulis, G.A., Belibassakis, K.A., Gerostathis, Th.P., Kapelonis, Z.G., 2014. Application of SWAN wave model for climatic simulation of sea condition at coastal areas of the Mediterranean. In: 6th Panhellenic Conf. Coastal Zones Manage. Improvement, 24—27 November 2014, Athens, Greece, 345—364.

Athanassoulis, G.A., Belibassakis, K.A., Gerostathis, Th.P., Kapelonis, Z.G., 2015. Wave climate analysis in the Mediterranean Sea based on wave model simulation driven by climatological winds. Technical Report WP 2.2. Res. Program CCSEAWAVS. (in Greek).

Benoit, M., Marcos, F., Becq, F., 1996. Development of a third generation shallow-water wave model with unstructured spatial meshing. In: 25th Int. Conf. Coastal Eng., Orlando, 465—478.

Booij, N., Ris, R.C., Holthuijsen, L.H., 1999. A third-generation wave model for coastal regions: 1. Model description and validation. J. Geophys. Res. 104 (C4), 7649—7666, http://dx.doi.org/10.1029/98JC02622.

Bouziotas, D., Rozos, E., Makropoulos, C., 2015. Water and the city: exploring links between urban growth and water demand management. J. Hydroinform. 17 (2), 176—192, http://dx.doi.org/10.2166/hydro.2014.053.

Breilh, J.-F., Bertin, X., Chaumillon, E., Giloy, N., Sauzeau, T., 2014. How frequent is storm-induced flooding in the central part of the Bay of Biscay? Global Planet. Change 122, 161—175, http://dx.doi.org/10.1016/j.gloplacha.2014.08.013.

Bretschneider, C.L., 1952. Revised wave forecasting relationships. In: Proc. 2nd Int. Conf. Coast. Eng., ASCE, Council Wave Res., Eng. Foundation, Berkeley, CA, 1—5.

Bretschneider, C.L., 1958. Revisions in wave forecasting: deep and shallow water. In: Proc. 6th Int. Conf. Coast. Eng., Council on Wave research, University of California, Richmond, CA, 30—67.

CEM, 2008. Coastal Engineering Manual. Coast. Eng. Res. Centre, US Army Corps Eng., Vicksburg, Mississippi, Part II, Chapter 2, 37—50; Chapter 4, 14—19.

Chini, N., Stansby, P.K., 2012. Extreme values of coastal wave overtopping accounting for climate change and sea level rise. Coast. Eng. 65, 27—37, http://dx.doi.org/10.1016/j.coastaleng.2012.02.009.

De Michele, C., Salvadori, G., Passoni, G., Vezzoli, R., 2007. A multivariate model of sea storms using copulas. Coast. Eng. 54 (10), 734—751, http://dx.doi.org/10.1016/j.coastaleng.2007.05.007.

Dean, R.G., Dalrymple, R.A., 2004. Coastal Processes with Engineering Applications. Cambridge Univ. Press, 488 pp.

DHI, 2007a. MIKE 21Boussinesq waves module: Scientific doc. Danish Hydraul. Instit., 1—24, (in Danish).

DHI, 2007b. MIKE 21Parabolic Mild Slope module: Scientific doc. Danish Hydraul. Instit., 1—22.

DHI, 2007c. MIKE 21Flow Model, HydroDynamic module: Scientific doc. Danish Hydraul. Instit., 1—60.

Dolan, R., Davis, R.E., 1992. An intensity scale for Atlantic coast northeast storms. J. Coast. Res. 8 (4), 840—853, http://www.jstor.org/stable/4298040.

Dolan, R., Davis, R.E., 1994. Coastal storm hazards. J. Coast. Res. (SI 12), 103—114, http://www.jstor.org/stable/25735593.

EurOtop Manual, 2007. In: Allsop, N.W.H., Pullen, T., Bruce, T., van der Meer, J.W., Schüttrumpf, H., Kortenhaus, A (Eds.), Overtopping Manual; Wave Overtopping of Sea Defences and Related Structures — Assessment Manual, http://www.overtopping-manual.com/manual.html (accessed 10 December 2015).

Evers, M., Jonoski, A., Maksimovic, C., Lange, L., Ochoa, S., Dinkneh, A.J., Cortés, Almoradie, A., van Andel, S.J., Simoes, N., Wang, L. P., Makropoulos, C., 2012. Collaborative modelling for active involvement of stakeholders in urban flood risk management. Nat. Hazards Earth Syst. Sci. 12 (9), 2821—2842, http://dx.doi.org/10.5194/nhess-12-2821-2012.

Galanis, D., 2010. Registration and control of the meteorological facts of the Meteorogical Station of Chania. (Dipl. Thesis). Tech. Edu. Instit. Chania, http://nefeli.lib.teicrete.gr/browse/sefe/sdfp/2010/GalanisDimitrios/attached-document-1277730043-268059-19836/2010galanis.pdf (accessed 10 December 2015).

Gallien, T.W., Sanders, B.F., Flick, R.E., 2014. Urban coastal flood prediction: integrating wave overtopping, flood defenses and drainage. Coast. Eng. 91, 18—28, http://dx.doi.org/10.1016/j.coastaleng.2014.04.007.

GEBCO, 2009. Gridded Global Bathymetry Data. British Oceanographic Data Centre, Liverpool, https://www.bodc.ac.uk/data/online_delivery/gebco/ (accessed 10 December 2015).

Halsey, S.D., 1986. Proposed Classification Scale for Major Northeast Storms: East Coast USA, Based on Extent of Damage. Geol. Soc. Am., abstracts with programs (Northeastern section), 18, 21 pp.

Karambas, T.V., 2015. Modelling of climate change impacts on coastal flooding/erosion, ports and coastal defence structures. Desalinat. Water Treat. 54 (8), 2130—2137, http://dx.doi.org/10.1080/19443994.2014.934115.

Koftis, T.H., Prinos, P., Galiatsatou, P., Karambas, Th., 2015. An integrated methodological approach for the upgrading of coastal

structures due to climate effects. In: E-proceedings of the 36th IAHR World Conference, 28 June—3 July, The Hague, the Netherlands.

Kokkinos, D., Prinos, P., Galiatsatou, P., 2014. Assessment of coastal vulnerability for present and future climate conditions in coastal areas of the Aegean Sea. In: Paper Presented at the 11th International Conference on Hydroscience & Engineering: Hydro-Engineering for Environmental Challenges, http://www.thalis-ccseawavs.web.auth.gr/el/publications (accessed 10 December 2015).

Kundzewicz, Z.W., 2014. Adapting flood preparedness tools to changing flood risk conditions: the situation in Poland. Oceanologia 56 (2), 385—407, http://dx.doi.org/10.5697/oc.56-2.385.

Laudier, N.A., Thornton, E.B., MacMahan, J., 2011. Measured and modeled wave overtopping on a natural beach. Coast. Eng. 58 (9), 815—825, http://dx.doi.org/10.1016/j.coastaleng.2011.04.005.

Li, F., van Gelder, P.H.A.J.M., Ranasinghe, R., Callaghan, D.P., Jongejan, R.B., 2014. Probabilistic modelling of extreme storms along Dutch coast. Coast. Eng. 86, 1—13, http://dx.doi.org/10.1016/j.coastaleng.2013.12.009.

Long, J.W., Bakker, A.T.M., de Plant, N.G., 2014. Scaling coastal dune elevation changes across storm-impact regimes. Geophys. Res. Lett. 41 (8), 2899—2906, http://dx.doi.org/10.1002/2014GL059616.

Lynett, P., Melby, J., Kim, D., 2010. An application of Boussinesq modeling to Hurricane wave overtopping and inundation. Ocean Eng. 37 (1), 135—153, http://dx.doi.org/10.1016/j.oceaneng.2009.08.021.

Majewski, D., Schrodin, R., 1994. Short description of the Europa-Modell (EM) and Deutschland-Modell (DM) of the DWD. Quarterly Bull. 1—31.

Makropoulos, Ch., Tsoukala, V.K., Belibassakis, K., Lykoy, A., Chondros, M., Gougoura, P., 2015. Managing flood risk in coast cities through an integrated modelling framework supporting stakeholders' involvement: the case study of Rethymno. In: E-proceedings of the 36th IAHR World Conference, 28 June—3 July, The Hague, the Netherlands.

Makropoulos, Ch., Tsoukala, V.K., Lykou, A., Chondros, M., Manojlovic, N., Vojinovic, Z., 2014. Extreme and rare events in coastal regions due to climate change — a case study application in Rethymno. In: Int. Conf. ADAPTto CLIMATE. 27—28 March 2014, Nicosia, Cyprus (e-proceedings: http://adapttoclimate.uest.gr/index.php/proceedings1, last accessed 10 December 2015).

Matias, A., Williams, J.J., Masselink, G., Ferreira, O., 2012. Overwash threshold for gravel barriers. Coast. Eng. 63, 48—61, http://dx.doi.org/10.1016/j.coastaleng.2011.12.006.

McCabe, M., Stansby, P.K., Rogers, B.D., Cunningham, L.S., 2014. Boussinesq modelling of tsunami and storm wave impact. Proc. Inst. Civil Eng. — Eng. Comput. Mech. 167 (3), 106—116, http://dx.doi.org/10.1680/eacm.13.00025.

Mendoza, E.T., Jiménez, J.A., 2009. Regional vulnerability analysis of Catalan beaches to storms. Proc. Inst. Civil Eng. — Mar. En. 162 (3), 127—135, http://dx.doi.org/10.1680/maen.2009.162.3.127.

Mendoza, E.T., Jiménez, J.A., 2006. Storm-induced beach erosion potential on the Catalonian Coast. J. Coast. Res. SI 48 (Proc. 3rd Spanish Conf. Coast. Geomorphol.), 81—88, http://www.jstor.org/stable/25737386.

Mendoza, E.T., Jiménez, J.A., Mateo, J., 2011. A coastal storms intensity scale for the Catalan sea (NW Mediterranean). Nat. Hazards Earth Syst. Sci. 11 (9), 2453—2462, http://dx.doi.org/10.5194/nhess-11-2453-2011.

Mendoza, E.T., Trejo-Rangel, M.A., Salles, P., Appendini, C.M., González, J.L., Torres-Freyermuth, A., 2013. Storm characterization and coastal hazards in the Yucatan Peninsula. J. Coast. Res. SI 65, 790—795.

Oumeraci, H., Kortenhaus, A., Burzel, A., Naulin, M., Dassanayake, D.R., Jensen, J., Wahl, T., Mudersbach, C., Gönnert, G., Gerkensmeier, A.B., Fröhle, P., Ujeyl, G., 2015. XtremRisK — integrated flood risk analysis for extreme storm surges at open coasts and in estuaries: methodology, key results and lessons learned. Coast. Eng. J. 57 (1), 23 pp., http://dx.doi.org/10.1142/s057856341540001x.

Plant, N.G., Stockdon, H.F., 2015. How well can wave runup be predicted? Comment on Laudier et al. (2011) and Stockdon et al. (2006). J. Coast. Eng. 102, 44—48, http://dx.doi.org/10.1016/j.coastaleng.2015.05.001.

Prinos, P., 2014. Climate change effects on the Greek seas and coastal areas — the research project THALIS-CCSEAWAVS. In: 6th Panhellenic Conference on Coastal Zones Management and Improvement, 24—27 November 2014, Athens, 315—324.

Rangel-Buitrago, N., Anfuso, G., 2011. An application of Dolan and Davis (1992) classification to coastal storms in SW Spanish littoral. J. Coast. Res. SI 64, 1891—1895.

Ris, R.C., Holthuijsen, L.H., Booij, N., 1999. A third-generation wave model for coastal regions: 2. Verification. J. Geophys. Res. 104 (C4), 7667—7681, http://dx.doi.org/10.1029/1998JC900123.

RISC-KIT, 2015. Coastal Hazard Assessment Module, Deliverable No: D.2.1, Ref.: WP2 - Task 2.1, 113 pp., http://www.risckit.eu/np4/file/23/RISCKIT_D.2.1_Coastal_Hazard_Asssessment.pdf.

Saffir, H.S., 1977. Design and Construction Requirements for Hurricane Resistant Construction. ASCE, New York, Preprint No. 2830, 20 pp.

Senechal, N., Coco, G., Bryan, K.R., Holman, R.A., 2011. Wave runup during extreme storm conditions. J. Geophys. Res. 116 (C7), C07032, http://dx.doi.org/10.1029/2010JC006819.

Simpson, R.H., 1979. A proposed scale for ranking hurricanes by intensity. In: Minutes of the Eighth NOAA, NWS Hurricane Conference, Miami.

Smith, R., Bates, P., Hayes, D., 2012. Evaluation of a coastal flood inundation model using hard and soft data. Environ. Modell. Softw. 30, 35—46, http://dx.doi.org/10.1016/j.envsoft.2011.11.008.

Stockdon, H.F., Holman, R.A., 2011. Observations of wave runup, setup, and swash on natural beaches. USGS Data Ser. 602, http://pubs.usgs.gov/ds/602/ (accessed 10 December 2015).

Stockdon, H.F., Holman, R.A., Howd, P.A., Sallenger, A.H., 2006. Empirical parameterization of setup, swash, and runup. Coast. Eng. 53 (7), 573—588, http://dx.doi.org/10.1016/j.coastaleng.2005.12.005.

Velikou, K., Tolika, K., Anagnostopoulou, C., Tegoulias, I., Vagenas, C., 2014. High resolution climate over Greece: assessment and future projections. In: 12th International Conference on Meteorology, Climatology and Atmospheric Physics (COMECAP 2014), Heraklion.

WAMDI-Group, 1988. The WAM model — a third generation ocean wave prediction model. J. Phys. Oceanogr. 18 (12), 1775—1810, http://dx.doi.org/10.1175/1520-0485(1988)018<1775:twmtgo>2.0.co;2.

Warner, N., Tissot, P.E., 2012. Storm flooding sensitivity to sea level rise for Galveston Bay, Texas. Ocean Eng. 44, 23—32, http://dx.doi.org/10.1016/j.oceaneng.2012.01.011.

Williams, J.A., Flather, R.A., 2004. The Operational Storm Surge Model: maintenance, performance and development, January 2003—March 2004. Proudman Oceanogr. Lab., Internal Doc. No. 164, 68 pp.

Wiśniewski, B., Wolski, T., 2011. Physical aspects of extreme storm surges and falls on the Polish coast. Oceanologia 53 (1—TI), 373—390, http://dx.doi.org/10.5697/oc.53-1-TI.373.